ISSN: 2414-1895 DOI: 10.6919/ICJE.202604_12(4).0040

Functionalized Graphene-Promoted Photocured Waterborne Acrylic/Polyaniline Conductive Anticorrosion Coatings

Hui Sun

University of Shanghai for Science and Technology, Shanghai 200000, China

Abstract

Poor compatibility between graphene and polymer matrices impedes composite coatings from simultaneously meeting bipolar-plate performance requirements for conductivity and corrosion resistance. To address this, a two-step graphene functionalization was developed that retains high electrical conductivity while enabling the graphene to participate in the photocuring reaction and thereby strengthen interfacial bonding with the resin. A ternary composite containing 71wt% functionalized graphene (FG) and 11.8wt% polyaniline (PANI) exhibited a high electrical conductivity of 124.9 S·cm^{-1} and a low interfacial contact resistance (ICR) of 16.18 mΩ·cm^2. Increasing the crosslink density between FG and the waterborne acrylic resin (WAR) reduced the corrosion current density (I_{corr}) to 0.56 μA·cm^{-2}. Property characterization indicates that PANI performs a dual role in the composite: it cooperates with FG to form continuous conductive pathways and fills coating voids while passivating the substrate, thereby enhancing barrier performance.

Keywords

Functionalized Graphene; Photocuring; Polyaniline; Composite Coating; Electrical Conductivity; Corrosion Protection.

1. Introduction

Driven by carbon-reduction policies and energy transition initiatives, clean and low-carbon energy technologies are progressively replacing conventional energy sources. Proton exchange membrane fuel cells (PEMFCs) convert chemical energy to electrical energy with high efficiency and generate water as the only major product, making them attractive for low-emission power generation. Bipolar plates (bps) are critical PEMFC components that provide electronic conduction and mechanical support [1]; they therefore require both high electrical conductivity and robust corrosion resistance. Typical targets for bps coatings are electrical conductivity >100 S·cm^{-1} and corrosion current density I_{corr} <1 μA·cm^{-2} under sulfuric acid conditions at pH = 3 and 80 °C [[2],[3]]. Metallic bps, especially stainless steels, are widely used because of their good electrical and thermal conductivity and manufacturability [4]. To improve the corrosion resistance of metallic bps in acidic environments, conductive anticorrosion coatings are commonly applied. Compared with noble-metal, amorphous carbon, and conductive ceramic coatings, polymer-based coatings are advantageous due to simple processing and low cost [[5]-[7]]. However, the inherently limited conductivity of polymers usually prevents standalone polymer coatings from meeting bps requirements; thus highly conductive carbon fillers are often incorporated to form percolating conductive networks.

Waterborne acrylic resins (WAR) undergo polymerization under UV irradiation to form crosslinked networks; they produce dense coatings with good chemical resistance and adhesion, making them a favorable polymer matrix for dispersing conductive fillers. Graphene, with its high aspect ratio and excellent conductivity, is frequently used to build continuous conductive networks and improve the physical barrier function of protective coatings [[8]-[10]]. Achieving target performance often

ISSN: 2414-1895 DOI: 10.6919/ICJE.202604_12(4).0040

requires graphene loadings above 50wt% [[11]-[14]], which can promote particle agglomeration, create interfacial defects, and reduce coating compactness, all of which undermine corrosion resistance. Surface functionalization is therefore an important strategy to improve graphene's water dispersibility and compatibility with polymers [[15],[16]].

Polyaniline (PANI) is a representative conductive polymer that provides electronic conduction via its conjugated backbone and can promote formation and repair of passive films on metal surfaces through reversible redox behavior, thus inhibiting localized corrosion propagation [[17]-[22]]. Nevertheless, conventionally synthesized PANI typically exhibits relatively low conductivity (10^{-3}–10^{1} $S \cdot cm^{-1}$) [[23],[24]], poor water dispersibility, and porous morphologies after polymerization that can facilitate electrolyte ingress [25]. These limitations hinder its use alone as the conductive anticorrosion phase for bps. Therefore, combining functionalized graphene (FG) and PANI as co-fillers in a WAR matrix is an attractive approach: microscopically they can form interpenetrating conductive pathways that raise bulk conductivity, while improving coating compactness and substrate adhesion and providing PANI's electrochemical passivation functionality to suppress electrochemical activity.

In this work, we fabricated FG/PANI/WAR composite coatings in which high-loading graphene was hydrophilized and functionalized with photocuring-active groups to improve dispersion, crosslink density, and interfacial bonding. PANI particles were homogeneously dispersed as a secondary conductive phase that, together with graphene, constructs an effective conductive network and, through its redox properties, enhances corrosion resistance under high-temperature acidic conditions. We systematically investigated the effects of graphene functionalization and PANI incorporation on the conductivity and corrosion performance of coatings for stainless-steel bps.

2. Methods

2.1 Two-step Functionalization for FG Preparation

Preparation of carboxylated graphene (CG) was performed via two consecutive reactions: diazotization and arylation. Briefly, 8.0 g p-aminobenzoic acid was dissolved in 480 mL deionized water and acidified with hydrochloric acid to pH 1.5. Under ice-bath cooling (0-5 °C) and light-excluded conditions, a 7.4wt% aqueous sodium nitrite solution was added dropwise to the p-aminobenzoic acid solution; after stirring for 1 h the diazonium salt solution was obtained. Multilayer graphene nanoplatelets and sodium cholate were added to deionized water at a mass ratio of 10:1, stirred and sonicated for 30 min to yield a graphene dispersion of 6.67 $mg \cdot mL^{-1}$. The diazonium solution and the graphene dispersion were then mixed and subjected to ultrasonic reaction at 60 °C for 8 h. The resulting mixture was repeatedly vacuum-filtered to obtain CG.

For subsequent grafting, 800 mg CG was dispersed in deionized water to a concentration of 2 $mg \cdot mL^{-1}$. 1-Ethyl-3-(3-dimethylaminopropyl) carbodiimide and N-hydroxysuccinimide were added at a molar ratio of EDC:NHS = 1:1.5 and the mixture was magnetically stirred for 1 h to activate the carboxyl groups. D-allylglycine (CG:D-allylglycine mass ratio = 1:1) was then introduced into the CG dispersion. The suspension was purged with nitrogen for 1 h and stirred at room temperature for 12 h. After multiple vacuum filtrations, D-allylglycine-modified carboxylated graphene (DCG) was obtained. The preparation routes for CG and DCG are summarized in Fig. 1.

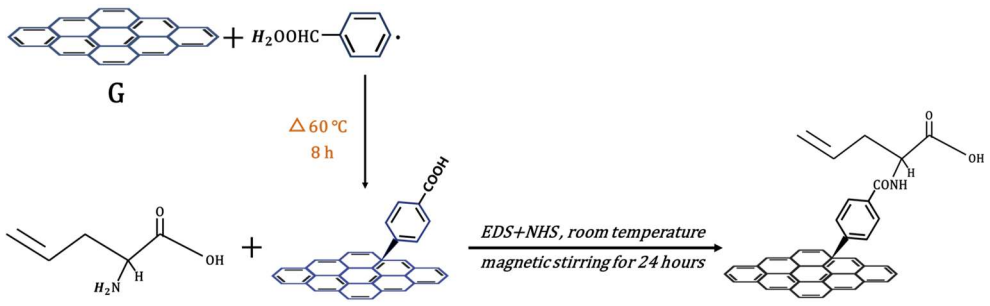

Figure 1. Preparation of CG and DCG.

ISSN: 2414-1895 DOI: 10.6919/ICJE.202604_12(4).0040

2.2 PANI Conductive Particle Synthesis

PANI particles were prepared via a chemical polymerization-dedoping-ball milling–re-doping procedure. Aniline and ammonium persulfate were used at a molar ratio of 1:1; the dopant acid for polymerization was 1 M H_2SO_4. Aniline and ammonium persulfate were each dispersed in the sulfuric acid solution and the mixture was stirred for 6 h to complete polymerization. The resulting PANI powder was vacuum-dried, then dispersed in 0.5 M NaOH and sonicated for 1 h to effect dedoping. To reduce particle size, the dedoped powder was ball-milled at 400 rpm for 12 h and collected by sieving. Finally, the ball-milled PANI was re-doped by soaking in a 10wt% camphorsulfonic acid solution with 1 h sonication, followed by filtration, washing, and drying.

2.3 Composite Coating Preparation

Two sets of FG/PANI/WAR composite coatings were prepared by bar coating. The first set comprised DCG/WAR binary coatings with DCG contents of 65, 67, 69, 71, 73 and 75wt%. Based on the performance evaluation of the first set, the composition showing the best overall properties was selected as the baseline; to that formulation, PANI was added at 2, 4, 6, 8 and 10 mg to produce a series of ternary FG/PANI/WAR coatings.

2.4 Characterization and Testing

The FG structure was characterized by Fourier transform infrared spectroscopy (FTIR) and Raman spectroscopy. Electrical conductivity of FG and the composite coatings was measured using an RTS-9 four-point probe system. Electrochemical polarization tests (PDP) were conducted on a PARSTAT 4000 A potentiostat. An 80 °C, pH 3 H_2SO_4 solution served as the electrolyte; coated 316L stainless steel, Ag/AgCl and platinum electrodes were used as the working, reference and counter electrodes, respectively, forming a three-electrode cell. Interfacial contact resistance (ICR) between the composite coating and the gas diffusion layer was measured under a compressive load of 1.38 MPa using a hydraulic press coupled with a digital milliohm meter, both before and after potentiostatic polarization (PSP). Coating adhesion and wettability were evaluated using an A-TM pull-off adhesion tester and a contact-angle goniometer, respectively.

3. Results and Discussion

3.1 Characterization of FG

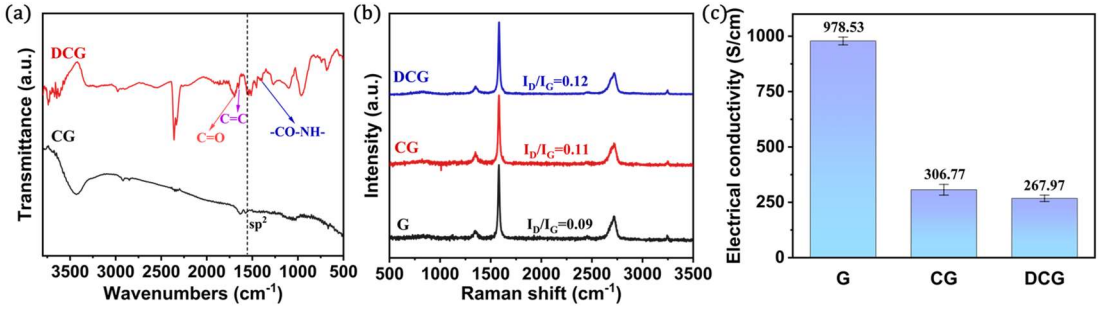

Figure 2. (a) FTIR spectra, (b) Raman spectra and (c) electrical conductivity of FG.

Figure 2(a) presents the FTIR spectra of CG and DCG. In the CG spectrum, characteristic bands assigned to -OH, carbonyl (C=O), and C=C (indicative of sp^2 domains) appear at ~3430, 1630 and 1570 cm^{-1}, respectively. The C=O band confirms successful grafting of carboxyl groups (-COOH) onto the graphene surface, while the persistent C=C band indicates limited functionalization and preservation of the graphene conjugated network. The DCG spectrum shows additional changes: a C-N (amide) feature at 1402 cm^{-1} and a C=O stretching band at 1700 cm^{-1} attributable to the carboxyl groups on the D-allylglycine chain. The absorption at 1650 cm^{-1} corresponds to C=C bonds introduced by D-allylglycine rather than the native sp^2 graphene network.

ISSN: 2414-1895 DOI: 10.6919/ICJE.202604_12(4).0040

Figure 2(b) shows the Raman spectra of G, CG and DCG. The D, G and 2D bands appear near ~1350, ~1580 and ~2700 cm^{-1}, corresponding to defect-induced vibrations of sp^2 carbon, the in-plane stretching of sp^2 carbon atoms, and the second-order two-phonon scattering of graphene, respectively. The ID/IG ratios for G, CG and DCG are 0.09, 0.11 and 0.12; the increasing ratio with carboxylation and D-allylglycine grafting indicates a rise in structural defects and partial conversion from sp^2 to sp^3 hybridization.

As shown in Figure 2(c), the disruption of the sp^2 network leads to decreased electrical conductivity. Carboxylation reduces the conductivity of pristine graphene from 978.53 to 306.77 $S \cdot cm^{-1}$, and subsequent grafting with D-allylglycine further lowers it to 267.97 $S \cdot cm^{-1}$, which nevertheless remains above the bipolar plate requirement (>100 $S \cdot cm^{-1}$). The two-step modification therefore sacrifices some conductivity while improving graphene's hydrophilicity and interfacial compatibility.

3.2 DCG/WAR Composite Coatings

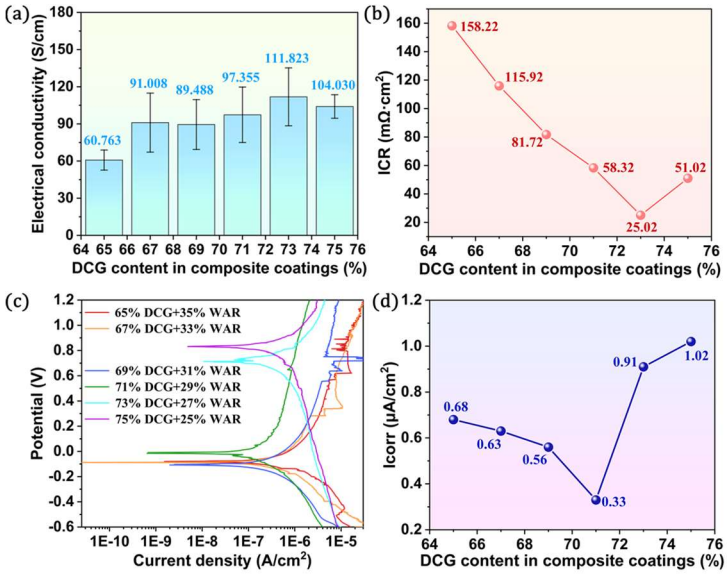

Figure 3. (a) Conductivity, (b) ICR, (c) PDP curves, and (d) I_{corr} of DCG/WAR composite coatings with varying DCG content.

Figure 3 shows the conductivity, ICR and I_{corr} of DCG/WAR composite coatings as a function of DCG content. The DCG/WAR system displays a clear optimum composition: conductivity increases from 60.76 $S \cdot cm^{-1}$ at low DCG content to a maximum of 111.82 $S \cdot cm^{-1}$ at 73% DCG, then decreases to 104.03 $S \cdot cm^{-1}$ with further DCG addition. This non-monotonic behavior reflects the evolution of the conductive network in the matrix: network continuity improves as DCG content increases and reaches an optimum, whereas excess conductive phase causes agglomeration and degrades the composite's conductivity. ICR follows a similar trend, dropping rapidly from 158.22 $m\Omega \cdot cm^2$ to a minimum of 25.02 $m\Omega \cdot cm^2$ before rising again to 51.02 $m\Omega \cdot cm^2$, consistent with initial densification of the conductive network followed by adverse effects from overloading the conductive phase. The C=C moieties grafted on the DCG surface can participate in the photopolymerization of the WAR resin; thus a moderate increase in DCG fraction strengthens interfacial bonding in the composite coating. According to the potentiodynamic polarization results (Fig. 3c), when DCG content is raised to 71% the I_{corr} decreases to 0.33 $\mu A \cdot cm^{-2}$, indicating excellent corrosion resistance; at this composition the coating also exhibits good conductivity (97.36 $S \cdot cm^{-1}$) and a relatively low ICR (58.32 $m\Omega \cdot cm^2$), representing the best overall performance.

To further clarify the effect of graphene functionalization, the performance of CG/WAR and DCG/WAR coatings with the same composition was compared. The 71%CG/29%WAR coating shows a conductivity of 86.23 $S \cdot cm^{-1}$, an ICR of 94.78 $m\Omega \cdot cm^2$ and an I_{corr} of 1.34 $\mu A \cdot cm^{-2}$, all inferior to the corresponding DCG/WAR coating. These differences align with the mechanism by

ISSN: 2414-1895 DOI: 10.6919/ICJE.202604_12(4).0040

which the D-allyl glycine–derived surface functionalities suppress graphene aggregation, improve compatibility with the WAR matrix and promote photopolymerization. The two-step modification of graphene extends conductive pathways, enhances interfacial adhesion and facilitates formation of a more uniform passive film, thereby inhibiting corrosion. Surface morphologies of the 71%DCG/29%WAR and 71%CG/29%WAR coatings are presented in Fig. 4. The 71%DCG/29%WAR coating exhibits fewer warped graphene sheets and voids, and is smoother and denser than the 71%CG/29%WAR coating, consistent with the corrosion test results. Enhanced dispersion and improved interfacial compatibility resulting from graphene functionalization aid the formation of a more continuous conductive network within the WAR matrix.

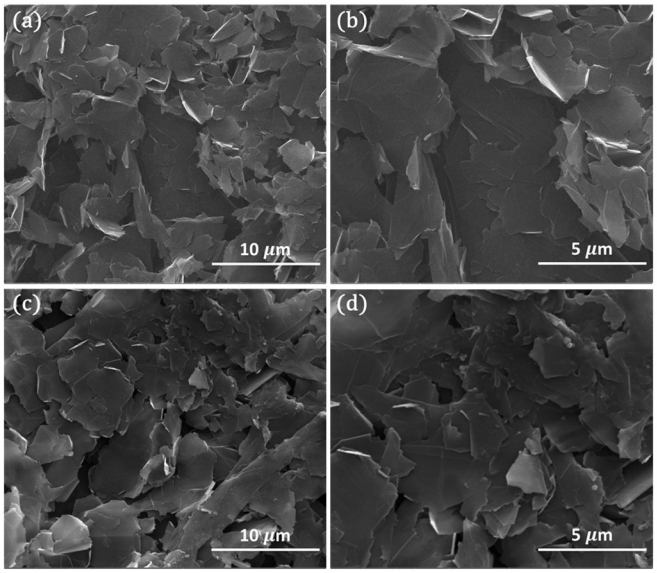

Figure 4. (a–b) Morphology of the 71% CG/29% WAR coating and (c–d) morphology of the 71% DCG/29% WAR coating.

Adhesion test results show that the CG/WAR coatings (Fig. 5a–b) exhibit low adhesion strengths of 0.30 MPa and 0.25 MPa at 71% and 73% CG content, respectively, whereas the DCG/WAR coatings (Fig. 5c–h) generally display higher and more stable adhesion. This behavior can be attributed to the effects of graphene functionalization on dispersion, interfacial compatibility, and the photopolymerization process. Polar functional groups introduced by grafting D-allyl glycine effectively suppress graphene sheet agglomeration and improve dispersion within the WAR matrix. In addition, C=C bonds on the graphene surface serve as co-reactive sites in photoinitiated free-radical polymerization, copolymerizing with the resin's unsaturated monomers to increase crosslink density and strengthen interfacial bonding. By contrast, CG/WAR coatings suffer from severe agglomeration, abundant surface defects and poor phase compatibility, which lead to inferior adhesion.

Figure 5. Adhesion strength of the composite coatings: (a) 71% CG / 29% WAR, (b) 73% CG / 27% WAR, (c) 65% DCG / 35% WAR, (d) 67% DCG / 33% WAR, (e) 69% DCG / 31% WAR, (f) 71% DCG / 29% WAR, (g) 73% DCG / 27% WAR, (h) 75% DCG / 25% WAR.

ISSN: 2414-1895 DOI: 10.6919/ICJE.202604_12(4).0040

In Figure 6a–e, the water contact angle gradually increases from 52.4° to 70.3°, but decreases to 60° when the DCG content reaches 75%. This behavior can be explained by two factors. First, at moderate DCG loadings the graphene disperses uniformly in the WAR matrix; surface functionalization improves interfacial compatibility with the resin, leading to exposure of hydrophobic graphene faces at the composite surface and an increase in macroscopic hydrophobicity. Second, at excessive DCG content sheet restacking or overlap readily occurs, degrading surface uniformity and exposing hydrophilic groups, which reduces the contact angle. Therefore, DCG/WAR coatings with 71-73% DCG achieve optimal hydrophobic performance and are most effective at suppressing the formation of electrochemical corrosion pathways.

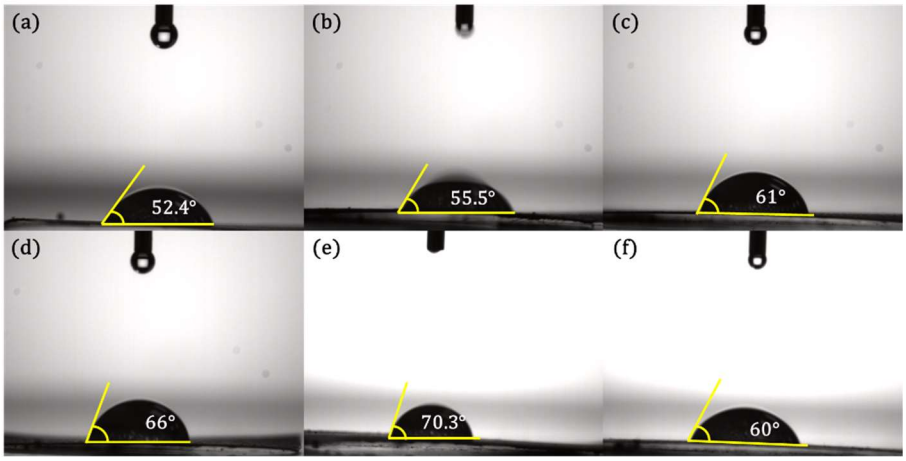

Figure 6. Water contact angles of DCG/WAR composite coatings: (a) 65% DCG / 35% WAR, (b) 67% DCG / 33% WAR, (c) 69% DCG / 31% WAR, (d) 71% DCG / 29% WAR, (e) 73% DCG / 27% WAR, (f) 75% DCG / 25% WAR.

3.3 DCG/PANI/WAR Ternary Composite Coatings

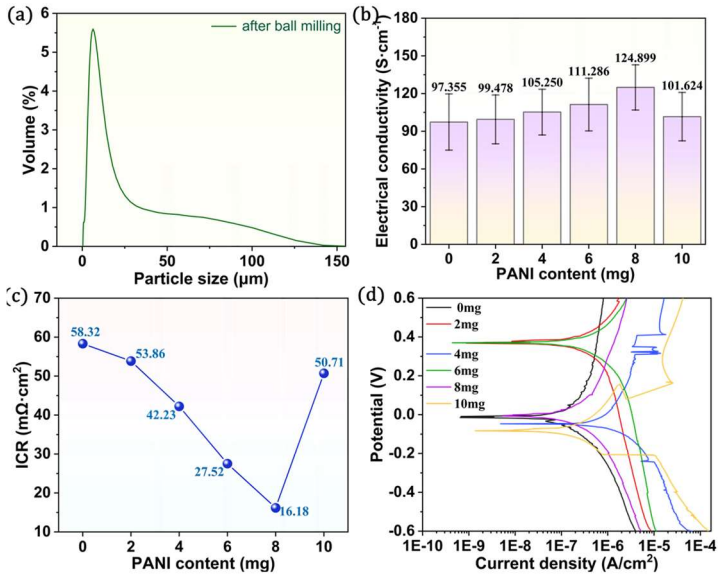

Figure 7. (a) Laser particle size distribution of PANI after ball milling; (b) electrical conductivity, (c) ICR and (d) PDP curves of DCG/PANI/WAR composite coatings with varying PANI loadings.

PANI particles used in the DCG/PANI/WAR ternary system were prepared by chemical polymerization, dedoping, ball milling and redoping, yielding an electrical conductivity of 32.8 $S \cdot cm^{-1}$ and an average particle diameter of 12.45 μm (Fig. 7a). The electrical conductivity, ICR and PDP curves of DCG/PANI/WAR coatings with varying PANI contents are presented in Fig. 7b–d. Both

ISSN: 2414-1895 DOI: 10.6919/ICJE.202604_12(4).0040

conductivity and ICR reach optimal values at a PANI addition of 8 mg, with a maximum conductivity of 124.9 $S \cdot cm^{-1}$ and a minimum ICR of 16.18 $m\Omega \cdot cm^2$. The results indicate that interfacial compatibility between WAR and DCG improves with increasing DCG content but declines beyond a critical loading owing to agglomeration and defect formation caused by excess DCG. Fitting of the PDP curves shows that I_{corr} follows an increase-decrease-increase trend, with a minimum I_{corr} of 0.56 $\mu A \cdot cm^2$ at 8 mg PANI. At this loading a continuous conductive pathway and barrier network are established within the matrix, yielding the best combined electrical conductivity and corrosion resistance; both lower and higher PANI loadings produce uneven distribution or agglomeration-related defects that impair coating densification.

4. Conclusion

To meet the performance requirements for metallic BPs in PEMFCs, a ternary conductive, corrosion-resistant coating was prepared by bar coating. Carboxylated graphene was mildly functionalized with D-allylglycine; the surface-grafted C=C groups participate in the free-radical polymerization of WAR without compromising graphene conductivity, thereby increasing crosslinking density. Small-particle, doped PANI was incorporated to form a continuous conductive network with the graphene and improve overall conductivity. When the PANI loading reached the critical value of 8 mg, a continuous conductive and barrier network was established, yielding a conductivity of 124.9 $S \cdot cm^{-1}$, an ICR of 16.18 $m\Omega \cdot cm^2$, and a I_{corr} of 0.56 $\mu A \cdot cm^2$.

References

[1] T. Wilberforce, Z. El-Hassan, E. Ogungbemi, O. Ijaodola, F.N. Khatib, A. Durrant, et al., A comprehensive study of the effect of bipolar plate (BP) geometry design on the performance of proton exchange membrane (PEM) fuel cells, Renew. Sustain. Energy Rev. 111 (2019) 236–260.

[2] T. Wilberforce, O. Ijaodola, E. Ogungbemi, F.N. Khatib, T. Leslie, Z. El-Hassan, et al., Technical evaluation of proton exchange membrane (PEM) fuel cell performance – A review of the effects of bipolar plates coating, Renew. Sustain. Energy Rev. 113 (2019) 109286.

[3] J.-H. Choi, H.E. Kang, D.-J. Kim, Y.S. Yoon, A comprehensive review of stainless-steel bipolar plate coatings and their role in mitigating corrosion in aggressive proton-exchange membrane fuel cells environments, Chem. Eng. J. 493 (2024) 152662.

[4] K. Xiong, W. Wu, S. Wang, L. Zhang, Modeling, design, materials and fabrication of bipolar plates for proton exchange membrane fuel cell: A review, Appl. Energy 301 (2021) 117443.

[5] R. Liu, Q. Jia, B. Zhang, Z. Lai, L. Chen, Protective coatings for metal bipolar plates of fuel cells: A review, Int. J. Hydrogen Energy 47 (2022) 22915–22937.

[6] P. Yi, D. Zhang, D. Qiu, L. Peng, X. Lai, Carbon-based coatings for metallic bipolar plates used in proton exchange membrane fuel cells, Int. J. Hydrogen Energy 44 (2019) 6813–6843.

[7] Y. Song, C. Zhang, C.-Y. Ling, M. Han, R.-Y. Yong, D. Sun, et al., Review on current research of materials, fabrication and application for bipolar plate in proton exchange membrane fuel cell, Int. J. Hydrogen Energy 45 (2020) 29832–29847.

[8] L. Syam Sundar, M. Amin Mir, M. Waqar Ashraf, F. Djavanroodi, Synthesis and characterization of graphene and its composites for Lithium-Ion battery applications: A comprehensive review, Alexand. Eng. J. 78 (2023) 224–245.

[9] X. Li, B. Li, Y. He, F. Kang, A review of graphynes: Properties, applications and synthesis, New Carbon Mater. 35 (2020) 619–629.

[10] J. Mu, F. Gao, G. Cui, S. Wang, S. Tang, Z. Li, A comprehensive review of anticorrosive graphene-composite coatings, Prog. Org. Coat. 157 (2021) 106321.

[11] J. Cui, J. Xu, H. Xiu, H. Wang, J. Li, J. Yang, Graphene-Dominated Hybrid Coatings with Highly Compacted Structure on Stainless Steel Bipolar Plates, ACS Appl. Mater. Interfaces 2022, 14, 37059–37067.

[12] F. Guo, J. Li, Facile production of graphene-based ternary composite coatings on metallic bipolar plates, Appl. Surf. Sci. 2024, 669, 160360.

ISSN: 2414-1895 DOI: 10.6919/ICJE.202604_12(4).0040

[13] Y. Qi, J. Cui, F. Guo, J. Li, Graphene/polyaniline waterborne composite coatings for metallic bipolar plates, Prog. Org. Coat. 2024, 197, 108829.

[14] C. Gong, J. Cui, Y. Sun, S. Shen, J. Li, Uniform electrodeposition of graphene/polypyrrole conductive coatings promoted by graphene quantum dots, Prog. Org. Coat. 2025, 204, 109269.

[15] Y. Wang, S. Li, H. Yang, J. Luo, Progress in the functional modification of graphene/graphene oxide: a review, RSC Adv. 2020, 10, 15328–15345.

[16] J. Cui, Y. Bao, Y. Sun, H. Wang, J. Li, Critical factors on corrosion protective waterborne coatings containing functionalized graphene oxide: a review, Compos. Part A 2023, 174, 107729.

[17] G. Liao, Q. Li, Z. Xu, The chemical modification of polyaniline with enhanced properties: A review, Prog. Org. Coat. 2019, 126, 35–43.

[18] M. Beygisangchin, S. A. Rashid, S. Shafie, A. R. Sadrolhosseini, H. N. Lim, Preparations, Properties, and Applications of Polyaniline and Polyaniline Thin Films-A Review, Polymers. 2021, 13, 2003.

[19] V. Babel, B. L. Hiran, A review on polyaniline composites: Synthesis, characterization, and applications, Polym. Compos. 2021, 42, 3142–3157.

[20] C. O. Baker, X. Huang, W. Nelson, R. B. Kaner, Polyaniline nanofibers: broadening applications for conducting polymers, Chem. Soc. Rev. 2017, 46, 1510–1525.

[21] H. Lgaz, H.-S. Lee, A.A. Alrashdi, M. Messali, Polyaniline-based hybrid coatings for corrosion protection: Breakthroughs in nanocomposite design, self-healing, and corrosion sensing, Polymer Test. 154 (2026) 109053.

[22] F. Gao, J. Mu, Z. Bi, S. Wang, Z. Li, Recent advances of polyaniline composites in anticorrosive coatings: A review, Prog. Org. Coat. 151 (2021) 106071.

[23] Y. Wang, Y. Wang, X. Xu, C. Wang, X. Gao, Controlled chemical oxidative polymerization of conductive polyaniline with excellent pseudocapacitive properties, J. Mater. Sci.: Mater. Electron. 2021, 32, 6965–6975.

[24] H. Nazari, R. Arefinia, An investigation into the relationship between the electrical conductivity and particle size of polyaniline in nano scale, Int. J. Polym. Anal. Charact. 2019, 24, 178–190.

[25] Y. Sun, C. Hu, J. Cui, S. Shen, H. Qiu, J. Li, Electrodeposition of polypyrrole coatings doped by benzenesulfonic acid-modified graphene oxide on metallic bipolar plates, Prog. Org. Coat. 170 (2022) 106995.